Vol. 38 — N° 4 12 14 P. 409–420

GEOSTANDARDS and GEOANALYTICAL RESEARCH

Determination of U–Pb Ages for Young Zircons using Laser Ablation-ICP-Mass Spectrometry Coupled with an Ion Detection Attenuator Device

Shuhei **Sakata** (1)*, Kentaro **Hattori** (1), Hideki **Iwano** (2), Takaomi D. **Yokoyama** (1), Tohru **Danhara** (2) and Takafumi **Hirata** (1)

(1) Laboratory for Planetary Sciences, Kyoto University, Kitashirakawa Oiwakecho, Sakyo-ku, Kyoto, 606-8502, Japan
(2) Kyoto Fission-Track Co. Ltd., Omiya, Kita-ku, Kyoto, 603-8832, Japan
* Corresponding author. e-mail: junchan@kueps.kyoto-u.ac.jp

We have developed new analytical procedures to measure precise and accurate ^{238}U–^{206}Pb and ^{235}U–^{207}Pb ages for young (~ 1 Ma) zircons using laser ablation-ICP-mass spectrometry. For young zircons, both careful correction for the background counts and analysis of very small Pb/U ratios (i.e., $^{206}Pb/^{238}U < 0.00016$ and $^{207}Pb/^{235}U < 0.0001$ for 1 Ma zircons) are highly desired. For the correction of the background, the contribution of the background signal intensities for the analytes, especially for the residual signal intensities for ^{206}Pb and ^{207}Pb, was defined through laser ablation of synthesised zircons (ablation blank) containing negligible Pb. The measured signal intensities for ^{202}Hg, ^{206}Pb and ^{207}Pb signals obtained by the ablation blank were slightly higher than those obtained by data acquisition without laser ablation (gas blank). For the wider dynamic range measurements on Pb/U ratios, an attenuator device for the ion detection system was employed to extend the capability to monitor high-intensity signals (i.e., > 3 Mcps). Through the attenuator device, the ion currents were reduced to 1/450 of the signal intensity without the attenuator. Because the switching time for the attenuator was shorter than 1 ms, signal intensities for only specific isotopes could be reduced. With attenuation of the ^{238}U signal, counting statistics on ^{206}Pb and ^{207}Pb isotopes could be improved and counting loss on the ^{238}U signal could be minimised. To demonstrate the reliability of this new analytical technique, ^{238}U–^{206}Pb and ^{235}U–^{207}Pb ages for three young zircon samples (collected from Osaka Group Pink Volcanic Ash, Kirigamine and Bishop Tuff) were measured. The data presented here demonstrate clearly that the present technique could become a major analytical tool for *in situ* U–Pb age determination of young zircons (~ 1 Ma).

Nous avons mis au point de nouvelles procédures d'analyse pour obtenir des mesure sprécises et exactes des âges ^{238}U-^{235}U-^{206}Pb et ^{207}Pb pour des zircons jeunes (~ 1 Ma) par spectrométrie de masse ICP couplée à un système d'ablation laser. Pour les jeunes zircons, des corrections précise sdu comptage du bruit de fond et des analyses des très faibles rapports Pb/U (i.e., $^{206}Pb/^{238}U$ <0,00016 et $^{207}Pb/^{235}U$ <0,0001 pour des zircons âgés d'1 Ma) sont très recherchés. Pour la correction du bruit de fond, la contribution de l'intensité de ce dernier pour les analytes, en particulier pour les intensités des signaux résiduels pour ^{206}Pb et ^{207}Pb, a été définie par l'ablation laser de zircons synthétisés (blanc d'ablation) contenant une quantité négligeable de Pb. Les intensités du signal mesurées pour les signaux de ^{202}Hg, ^{206}Pb et ^{207}Pb obtenue par ablation des blancs étaient légèrement supérieures à celles obtenues par l'acquisition de données sans ablation laser (gaz blanc). Pour les mesures de plage dynamique plus large sur les rapports Pb/U, un dispositif d'atténuation pour le système de détection des ions a été utilisé pour étendre la capacité de monitorer les signaux à haute intensité du signal (par exemple > 3 Mcps). Grâce au dispositif de l'atténuateur, les courants d'ions ont été réduits de 1/450 par rapport à l'intensité du signal sans atténuateur. Parce que le temps de commutation de l'atténuateur est inférieur à 1 ms, seules les intensités du signal d'isotopes spécifiques peuvent être réduites. Grace à l'atténuation du signal d'U^{238}, les statistiques de comptage sur les isotopes ^{206}Pb et ^{207}Pb pourraient être améliorées et la perte de comptage sur le signal d'U^{238}pourrait être minimisée. Pour démontrer la fiabilité de cette nouvelle technique analytique, les âges ^{238}U-^{235}U-^{206}Pb et ^{207}Pb de trois jeunes zircons (provenant des cendres volcaniques roses du Groupe d'Osaka etdes Tuffs de Kirigamine et de Bishop) ont été mesurés. Les données présentées dans cette études montrent

doi: 10.1111/j.1751-908X.2014.00320.x

GEOSTANDARDS and GEOANALYTICAL RESEARCH

Keywords: LA-ICP-MS, young zircon, geochronology, dynamic range.

Received 23 Apr 14 – Accepted 22 Jul 14

***clairement que la technique présentée pourrait devenir un outil analytique important pour la détermination in situ* de l'âge U-Pb des jeunes zircons (~ 1 Ma).**

Mots-clés : LA-ICP-MS, jeune zircon, datation U-Pb, plage dynamique, correction de base.

Laser ablation-ICP-mass spectrometry has become one of the most sensitive and rapid analytical tools for both multi-element concentration and isotope ratio measurements (Koch and Günther 2011). With improvements in the analytical sensitivity of the ICP-MS technique and also with better understanding of laser ablation phenomena, the resulting precision and accuracy of elemental and isotopic ratio measurements has been improved remarkably. This is well demonstrated in the U–Pb age determination for zircon or U-bearing minerals (e.g., Frei and Gerdes 2009, Iwano *et al.* 2013, Chew *et al.* 2014). With shorter wavelength or shorter pulse duration lasers, elemental fractionation during both laser ablation and ionisation has been significantly minimised (Guillong *et al.* 2003, Poitrasson *et al.* 2003, Horn and von Blanckenburg 2007, Freydier *et al.* 2008, Hirata and Kon 2008). Moreover, multi-collector-ICP-MS instruments provide higher-analytical precision in the measurement of $^{206}Pb/^{238}U$ and $^{207}Pb/^{235}U$ ratios (Bühn *et al.* 2009), so that the precision for *in situ* U–Pb age determination achieved by the LA-ICP-MS technique is now comparable to that obtained by secondary ion mass spectrometers (SIMS) (Košler *et al.* 2013). Despite the obvious success in obtaining precise $^{206}Pb/^{238}U$ and $^{207}Pb/^{235}U$ ratio measurements using LA-ICP-MS, several challenges associated with monitoring the small ^{206}Pb and ^{207}Pb signals still remain, especially in the case of age determinations of zircons of ~ 1 Ma or younger.

For young zircons, signal intensities for ^{206}Pb and ^{207}Pb isotopes are smaller than 100 cps, comparable to those found in background counts on ^{206}Pb and ^{207}Pb isotopes. It is widely recognised that background counts for ^{206}Pb and ^{207}Pb signals can vary significantly before and during laser ablation (e.g., Hirata and Nesbitt 1995, Iizuka and Hirata 2004). This could be due to the release of sample aerosols from the inside surface of the sample cell or tubing through the propagation of the laser shockwave, reflecting a 'Pb memory effect'. Also, ionisation conditions in the ICP can differ before and during sample introduction. For the gas blank, no sample aerosols are introduced into the ICP, whereas laser-induced sample aerosols are introduced into the ICP for the ablation blank. The 'mass loading' could change both the ionisation temperature and the plasma potential, resulting in differences in instrumental sensitivity for the ICP-MS system. To obtain reliable background counts for ^{206}Pb and ^{207}Pb isotopes, the background signal intensities should be measured under identical conditions during laser ablation of zircon samples. To achieve this, we measured background counts for analyses before and during laser ablation. Another important approach to minimise the contribution of possible changes in the background counts on ^{206}Pb and ^{207}Pb signals is to enhance the intensity of ^{206}Pb and ^{207}Pb signals from zircon samples. This could be achieved either by larger ablation pit sizes, higher energy fluence or by higher repetition rate of the laser emission. However, laser parameters that improve the intensity of ^{206}Pb and ^{207}Pb signals can also increase the signal intensity of ^{238}U. For zircons ~ 1 Ma and younger, using laser ablation conditions that produce a signal intensity for ^{206}Pb of > 1000 cps would result in a signal intensity for ^{238}U of $> 10^7$ cps, which could produce systematic errors in the $^{206}Pb/^{238}U$ and $^{207}Pb/^{235}U$ ratios due to counting loss of U ions. Moreover, detection of high-intensity ions can cause changes in gain and the white noise background (random noise) level of the multipliers. To minimise changes in the multiplier conditions and also to avoid possible erroneous measurements due to improper dead-time corrections for ^{238}U signals, the detection of high-intensity ion signals is not advisable. To overcome this, a new ion detector system utilising an attenuator device (Nu Instruments, Wrexham, UK) was employed for $^{206}Pb/^{238}U$ and $^{207}Pb/^{235}U$ ratio measurements. With the attenuator device, ion currents are passed through a metallic grid located in front of the multiplier, reducing their intensity to 1/450 of the level without the device. By using the attenuator, erroneous dead-time corrections and degradation of detection caused by high-intensity ion signals ($> 1 \times 10^6$ cps) can be avoided. Hence, only the ^{238}U signal is measured through the attenuator, and the other isotopes (^{202}Hg, $^{204}(Hg+Pb)$, ^{206}Pb, ^{207}Pb) can be measured without the attenuator. The time required for switching the attenuator is < 1 ms; hence, specific isotopes can be targeted for attenuation during fast mass scanning. To evaluate the short- to medium-term stability of the attenuator gain, attenuation of ^{238}U was

monitored for 10 hr. Possible dependence of attenuator gain on the signal intensity was also measured in this study. Reliability of the resulting $^{206}Pb/^{238}U$ and $^{207}Pb/^{235}U$ ratio data was evaluated through U–Pb age determinations of zircon samples of known ages.

Zircon samples

To investigate possible changes in background counts, background counts for ^{206}Pb and ^{207}Pb isotopes obtained without laser ablation (gas blank) and with laser ablation (ablation blank) were measured. Two zircons were used for the blank experiments. The first of these was collected from the Unzen-Fugendake volcano, Kyushu, Japan. The volcanic rock was produced during the last eruption in 1991, so the amounts of radiogenic ^{206}Pb and ^{207}Pb were assumed to be at negligible levels for the present analytical technique. The second was a synthesised zircon crystal that was grown in a MoO_3-Li_2MoO_4 flux according to the method of Chase and Osmer (1966) at 1250–900 °C (prepared by Dr. I. Shinno, Kyushu University, Japan), and also assumed to contain negligible Pb. The size of the resulting $ZrSiO_4$ crystal was about 2 mm.

To demonstrate the effect of the ablation blank protocol and Pb/U ratio measurements using the attenuator device, the ^{238}U–^{206}Pb and ^{235}U–^{207}Pb ages for three Quaternary zircons were measured, the ages of which were well known based on fission track (FT), Ar-Ar or U–Pb isotope dilution-thermal ionisation mass spectrometry (ID-TIMS) dating methods. The three zircons were sampled from the Osaka Group Pink (OGPK) Volcanic Ash, Osaka, Japan (Danhara *et al.* 1997), an obsidian from the Kirigamine area, Japan (Sugihara *et al.* 2009) and the Bishop Tuff, California, USA (Hildreth 1979). The reported ages are 1.00 ± 0.08 Ma (zircon fission-track age, Danhara *et al.* 1997) for OGPK; 0.94 ± 0.08 Ma (zircon fission-track age, Sugihara *et al.* 2009) for the Kirigamine zircons; and 0.7671 ± 0.0009 Ma (U–Pb zircon ID-TIMS age, Crowley *et al.* 2007), 0.7589 ± 0.0036 Ma (sanidine ^{40}Ar-^{39}Ar age, Sarna-Wojcicki *et al.* 2000) and 0.79 ± 0.04 Ma (zircon fission-track age: H. Iwano and T. Danhara, unpublished) for the Bishop Tuff zircons. The Bishop Tuff and Kirigamine zircons contain very high uranium concentrations: ~ 3000 μg g^{-1} for the Bishop Tuff and ~ 15000 μg g^{-1} for Kirigamine, whereas the OGPK zircon contains only 100 μg g^{-1} U.

Zircon samples were mounted in a PFA Teflon sheet (Danhara *et al.* 1993) on a hot plate (at 338 °C), and the surface was polished using diamond pastes with grit sizes of 3 μm and 1 μm. Prior to U–Pb isotopic determinations, possible surface contamination was further removed by pre-ablation with one laser shot (Iizuka and Hirata 2004).

Instrumentation and operational settings

A New Wave Research NWR193 laser ablation system (Fremont, CA 94538, USA) was used in this study. For the measurement of OGPK, ablation pit sizes of 25 μm (without attenuator) and 35 μm (with attenuator) were employed, with repetition rates of 8 Hz (without attenuator) and 10 Hz (with attenuator). For the Kirigamine and Bishop Tuff zircons, a pit size of 10 μm and repetition rates of 1–2 Hz (without attenuator) and 10 Hz (with attenuator) were used. A laser fluence of ~ 2.5 J cm^{-2} was used for the ablations. A high efficiency sample cell was used to minimise the washout time (Autrique *et al.* 2008). Helium instead of Ar was used as the carrier gas, which provided further improvement in the sample transport efficiency from the sample cell to the ICP and also minimised the re-deposition of the sample aerosol around the ablation pit (Eggins *et al.* 1998, Günther and Heinrich 1999, Jackson *et al.* 2004). Ablation conditions (fluence, pit size and repetition rate) were tuned to control the intensity of the ^{206}Pb, ^{207}Pb, ^{235}U and ^{238}U signals. The signal intensities for ^{206}Pb, ^{207}Pb and ^{238}U isotopes were optimised mainly by changing the pit size and laser repetition rate; laser fluence was kept constant to minimise possible changes in the magnitude of elemental fractionation during laser ablation. After some time (3 s) required for stabilising the signal intensities, no significant level of elemental fractionation of the Pb/U ratio was found for the first 12 s of ablation. The data acquisitions for all primary reference materials and samples were carried out under identical analytical conditions and, therefore, no correction for down-hole elemental fractionation was applied.

The ICP-MS instrument was a Nu Instruments (Wrexham, UK) AttoM high resolution-ICP-MS. To reduce the Hg background, a charcoal filter was applied to the Ar carrier gas (Hirata and Nesbitt 1995, Hirata *et al.* 2005). Commercially available charcoal granules especially designed for Hg adsorption were packed in the filter (Shirasagi No. 4, Activated Carbon, Japan Enviro Chemicals Co. Ltd., Osaka, Japan). Operational settings such as torch position, He and Ar gas flow rates and lens biases were tuned to maximise the intensity of ^{206}Pb and ^{238}U signals obtained by laser ablation of NIST SRM 610. Typical sensitivities using a pit size of 15 μm and a repetition rate of 8 Hz for NIST SRM 610 were 80000 cps for ^{206}Pb and 350000 cps for ^{238}U. Typical gas blank levels were 1300 cps for ^{202}Hg, 100 cps for ^{206}Pb and 80 cps for ^{207}Pb.

Great care was taken to minimise the production of oxide signals (i.e., UO^+ and ThO^+) and to reduce the measured instrumental mass bias of the $^{206}Pb/^{238}U$ ratio from the expected value for zircon 91500 (0.1792; Wiedenbeck *et al.* 1995). Low oxide production and minimal Pb/U bias were achieved with a shallow ion sampling depth (i.e., the distance between the ICP load coil and sampling cone). The shallow sampling depth resulted in a *ca.* 20% reduction in the ion transmission of the ICP-MS. Measured $^{208}Pb/^{232}Th$ ratios became closer to the literature values. Details of the instrumentation and operational settings are summarised in Table 1.

The $^{206}Pb/^{238}U$ ratio of the primary reference material zircon 91500 was measured four times – both before and after an analytical session in which 10–15 zircon samples were measured. The average $^{206}Pb/^{238}U$ ratio was calculated from eight total measurements of zircon 91500 and used for the correction of Pb/U fractionation in the other measured zircon samples. For the background corrections, signal intensities for the analytes were measured five times, both before and after an analytical session of ablated zircon samples, and both without laser ablation (gas blank) and with laser ablation of the Unzen and synthetic zircons (ablation blank). The averaged background counts were used for the blank subtraction corrections. Uncertainties from the Pb/U isotopic ratio measurements for zircon 91500, counting statistics for each analyte, and the measured attenuator gain were propagated to estimate the overall uncertainties for the resulting age data. The following equations were used for the propagation of errors for the $^{206}Pb/^{238}U$ and $^{207}Pb/^{235}U$ ratios:

$$(s_{Rel}^{Internal})^2 = (1/I_{Abs}^{isotope1}) + (1/I_{Abs}^{isotope2})^2 \quad (1)$$

$$(s_{Rel}^{Total})^2 = (s_{Rel}^{External})^2 + (s_{Rel}^{Internal})^2 + (s_{Rel}^{Gain})^2 \quad (2)$$

where Rel and Abs refer to mean relative and absolute values, respectively; $I^{isotope1}$ and $I^{isotope2}$ represent measured total counts of signal intensities for isotopes 1 (^{206}Pb, ^{207}Pb) and 2 (^{238}U, ^{235}U); and s^{Gain} is the standard deviation of the calibrated gain factor of the attenuation device.

Results and discussion

Ablation blank correction

The measured background counts for the ^{204}Pb, ^{206}Pb and ^{207}Pb isotopes could vary with laser ablation conditions. Figure 1 illustrates the resulting signal intensities for the gas blank, Unzen zircon and synthetic zircon after the background subtraction using the average gas blank measurements. The measured background counts for ^{206}Pb (Figure 1b) and ^{207}Pb (Figure 1c) signals obtained with the ablation blank were systematically higher than those obtained without laser ablation (gas blank). The obvious increase in the background counts for ^{206}Pb and ^{207}Pb isotopes could be explained by the release of sample aerosols either from inside the sample cell or from the transport tubing, possibly induced by the laser shockwave. This indicates clearly that reliable background correction could not be achieved by conventional gas blank corrections, especially for young zircons or zircons with very low U contents.

Scrutiny of the background counts for Pb reveals that the values for ^{206}Pb and ^{207}Pb obtained using the Unzen zircon were slightly higher than those obtained using the synthesised zircon crystal. The higher signal intensities from the Unzen zircon might be due to the incorporation of initial

Table 1.
Instrumentation and operational conditions

ICP mass spectrometer	
Instrument	AttoM (Nu Instruments, Wrexham, UK)
Scan mode	Deflector scan
Monitored isotope	^{202}Hg, $^{204}(Hg+Pb)$, ^{206}Pb, ^{207}Pb, ^{238}U
Dwell time	500 μs
Settling time	50 μs
Total integration time	12 s per run, 2.4 s for each mass peak. Total 12 s per run
Detector	Pulse counting
Dead time	12.2 ns
Attenuation gain	Calibrated by signal intensity of ^{238}U
Laser ablation	
Instrument	New Wave Research NWR193 (Fremont, CA 94538, USA)
Laser	ArF Excimer laser
Pulse duration	5 ns
Wavelength	193 nm
Typical fluence	2.5 J cm^{-2}
Repetition rate	1–8 Hz (without attenuator) 10 Hz (with attenuator)
Ablation pit size	
With attenuator	35 μm (for OGPK) 25 μm (for Kirigamine and Bishop Tuff)
Without attenuator	25 μm (for OGPK) 10 μm (for Kirigamine and Bishop Tuff)
Cell type	Two volume cell
Carrier gas	He 0.6 l min^{-1}
Make-up gas	Ar 0.9 l min^{-1}
Pre-ablation	3 s
Stabiliser	Enabled (150 ml) (Tunheng and Hirata 2004)
Background correction	Ablation blank using synthesised zircon crystal
Standardisation	
U-Pb dating	Zircon 91500 (natural)
Normalisation	$^{206}Pb/^{238}U$ = 0.17917 (zircon 91500) $^{238}U/^{235}U$ = 137.88
Common Pb correction	Not made

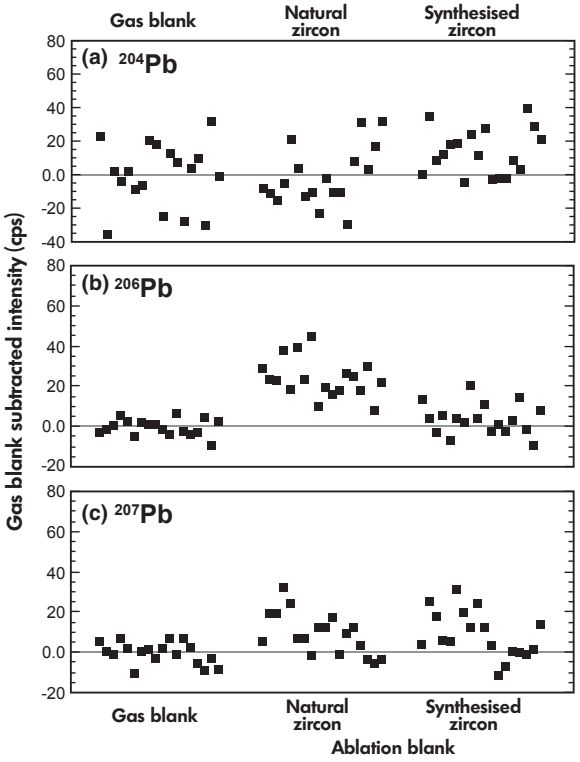

Figure 1. Background counts for ^{204}Pb, ^{206}Pb and ^{207}Pb isotopes obtained with and without laser ablation.

(common) Pb during crystallisation from its source melt, or by contribution of radiogenic Pb from short-lived nuclides in the U–Th decay series. However, the latter can be ruled out because the background counts for ^{207}Pb were almost comparable to those for ^{206}Pb (i.e., ^{207}Pb/^{206}Pb ~ 1). For zircons from the Unzen volcano, we believe that the background counts for ^{206}Pb and ^{207}Pb could be due to the initial distribution of common Pb during the crystallisation of zircon (i.e., $D^{Pb}_{Zircon/Magma} \neq 0$).

Counts of ^{204}Pb in the synthesised zircon were significantly higher than those in the gas blanks and Unzen zircon. Because there are no corresponding elevations in the measured intensities of ^{206}Pb and ^{207}Pb signals in the synthesised zircon, we believe that the elevated ^{204}Pb signal is the result of the isobaric interference of ^{204}Hg on ^{204}Pb. This suggests that the synthesised zircons suffered from the Hg contamination during synthesis. The comparison in the measured background counts in Figure 1 suggests that the best background correction might be achieved with ablation blank measurements of synthesised zircon crystals uncontaminated by Hg; unfortunately, such crystals were not available for our experiments. To overcome this, a silicon wafer could be used for the ablation blank. With our LA-ICP-MS set-up, the measured Hg background obtained with the ablation blank using the Si wafer was significantly lower than that obtained using the synthesised zircon. This suggests that ablation blanks using a Si wafer could provide reliable U–Pb age data, especially for samples for which common Pb corrections would be required.

Attenuator gain stability

Prior to the U–Pb isotopic age determination of zircon samples, we monitored the changes in attenuator gain through sequences (of 15–30 min duration) of zircon analyses. The gain of the attenuator device could be calculated from direct comparison of ^{238}U signal intensities obtained with the attenuator device and the signal intensity of ^{235}U without the device. The attenuator gain was defined by

$$G = R_{238U/235U}/(I_{238Uattn.}/I_{235U}) \quad (3)$$

where R represents the ^{238}U/^{235}U ratio (137.88, Cowan and Adler 1976), and $I_{238Uattn.}$ and I_{235U} represent the signal intensity for ^{238}U obtained through the attenuator device and the signal intensity of ^{235}U obtained without the attenuator device, respectively. In this study, the ^{235}U and ^{238}U signals were obtained from solution nebulisation of a 10 ng ml^{-1} U standard solution. The effect of instrumental drift was corrected by measuring the ^{238}U/^{235}U ratio of the same standard solution of 1 ng ml^{-1} concentration without the attenuator device before and after the measurement of gain stability over a period of 10 hr. No correction for the mass discrimination effect on the ^{235}U and ^{238}U isotopes was made, because we preferred to focus on possible time-dependent changes in attenuator gain through the measurements. Figure 2 illustrates the changes in attenuator gain over a 10 hr period. The average G-values for the first hour were used for normalisation, and relative changes in G-values (in %) were plotted against the analysis time. The random variation in the measured G-values (> 2%) was mainly due to the contribution from counting statistics from the attenuated ^{238}U and ^{235}U signals. Despite the large variation in each datum point, the gain of the present attenuator device showed a linear decrease with time of 0.11% hr^{-1}. This linear decrease may be explained either by small changes in the high-voltage supply to the ion lenses or by changes in the size of the grid for attenuation, through long-term sputtering by ions. Despite the obvious changes in the attenuator gain, its magnitude of change over the 10 hr period was ~ 1%. This suggests that drift in attenuator gain could be corrected by its careful calibration between the analytical sessions.

To test the dependence of attenuator gain on signal intensity under various laser ablation conditions (e.g., pit size,

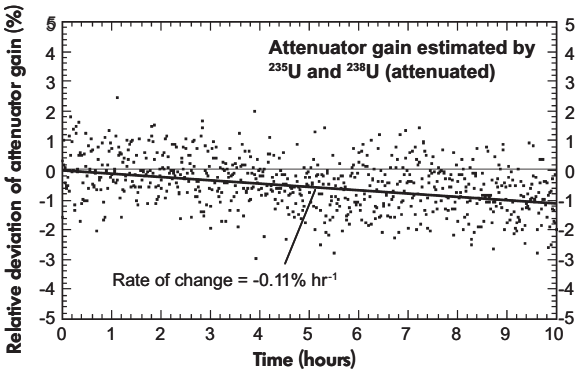

Figure 2. Time-dependent changes in attenuator gain calculated from the signal intensity of ^{235}U without attenuation and ^{238}U with attenuation. Values of the *y*-axis were normalised by the attenuator gain value obtained for the first hour.

fluence or repetition rate), the attenuator gain was calculated from different ^{238}U signal intensities derived from measurement of a standard solution. Figure 3 shows the measured $^{235}U/^{238}U$ ratio for a commercially available U tuning solution (CertiPrep XSTC-1252-100, lot number: 22-87 JB, Ltd., Middlesex, UK). The ^{238}U signal was monitored during the attenuation, whereas the signal intensity of the ^{235}U isotope was measured without the attenuator. The measured $^{235}U/^{238}U$ ratio was corrected by the separately calibrated attenuator gain ($G \sim 450$), and these were plotted against the calculated signal intensity of ^{238}U. No correction for the mass discrimination effect on U isotopes was made in this study, and only the relative deviation was evaluated. Error bars represent the uncertainties defined by two times the standard deviation calculated from 100 cycles of repeated analysis. The series of $^{235}U/^{238}U$ ratios demonstrates that the attenuator gain did not vary significantly until the ^{238}U ion current exceeded 100 Mcps, whereon it increased systematically with increasing count rates. In the U–Pb isotopic age determinations for the zircons in this study, the ^{238}U signal intensity did not exceed 100 Mcps, and therefore, no correction for the dependence of the attenuator gain on signal intensities was made. The data obtained in this study from the analysis of zircons revealed that both signal drift and intensity have negligible effects on changes in attenuator gain during the measurement of $^{206}Pb/^{238}U$ and $^{207}Pb/^{235}U$ ratios.

Attenuator gain was measured by comparing the measured signal intensities of ^{238}U obtained from laser ablation analysis of NIST SRM 610. The gain of the attenuator was calculated as the ratio of the ^{238}U signal intensity obtained without and with the attenuator device ($G = I_{w/o\ attn.}/I_{w\ attn.}$). The measured signal intensity and the resulting attenuator gain obtained by thirty repeat analyses are listed in Table 2. The average attenuator gain was 426.5 ± 7.5 (2*s*, n = 20). The uncertainty in this average is about 1.8%, which is comparable to or just smaller than the precision on the $^{206}Pb/^{238}U$ and $^{207}Pb/^{235}U$ ratio measurements made by LA-ICP-MS.

^{238}U–^{206}Pb and ^{235}U–^{207}Pb ages for zircons

To demonstrate the effect of the blank correction and attenuator device on the precision and accuracy of the U–Pb isotope ratio measurements, the $^{206}Pb/^{238}U$ and $^{207}Pb/^{235}U$ ratios for three natural zircons (OGPK, Bishop Tuff and Kirigamine) were measured. For the OGPK zircons,

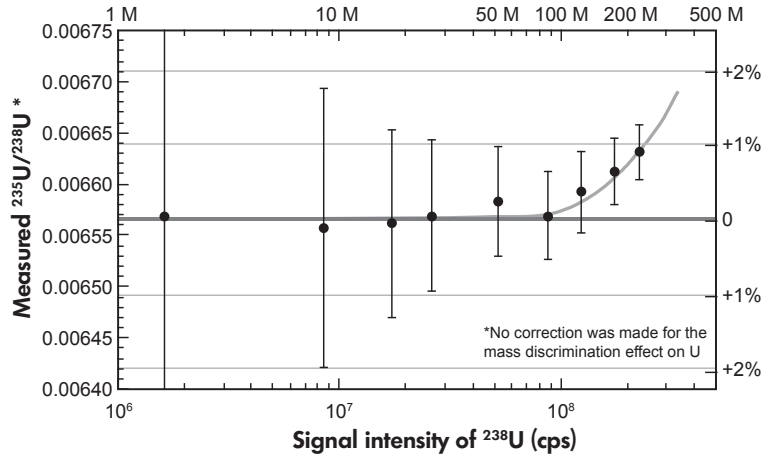

Figure 3. Effect of attenuator gain on the signal intensity of ^{238}U.

Table 2.
Attenuator gain found in ^{238}U signal obtained by laser ablation of NIST SRM 610

Run	Intensity of ^{238}U (cps)		Gain*
	w/o attenuation	with attenuation	
1	1041618	2429	428.9
2	1035046	2403	430.7
3	1049940	2483	422.9
4	1040996	2435	427.5
5	1033242	2439	423.7
6	1039420	2417	430.0
7	1027387	2418	424.9
8	1039802	2411	431.2
9	1018113	2386	426.8
10	1030842	2426	424.9
11	1014423	2415	420.0
12	1013077	2367	428.0
13	1009887	2384	423.6
14	1044557	2478	421.6
15	1012841	2336	433.6
16	990285	2322	426.5
17	985624	2333	422.6
18	998117	2354	424.0
19	1002392	2319	432.2
20	1031879	2417	427.0
		Mean	426.5
		2*s*	7.5
		% 2*s*	1.8

* Attenuation gain was defined as ratio of signal itensities obtained with and without attenuation ($I_{w/o\ attn}/I_{w\ attn}$).

the U–Pb isotope ratio data were obtained under three different conditions: (a) without the attenuator device and with a conventional gas blank correction; (b) with the attenuator device and with the gas blank correction procedure shown in Figure 1; and (c) with the attenuator device and with an ablation blank correction determined from the synthesised zircon. The resulting U–Pb isotopic data are listed in Table 3 and plotted in Figure 4.

Laser pit sizes and repetition rates were optimised to give a ^{238}U signal intensity of 10^6 cps for analyses that did not use the attenuator device. (Higher-signal intensities could produce systematic errors in age results due to improper dead-time correction for the pulse counting system.) The resulting signal intensity of ^{206}Pb was < 100 cps, and therefore, the measured $^{206}Pb/^{238}U$ and $^{207}Pb/^{235}U$ ratios were unreliable – mainly due to the poor counting statistics on ^{206}Pb and ^{207}Pb isotopes (Figure 4a). In fact, the resulting precisions of the $^{206}Pb/^{238}U$ and $^{207}Pb/^{235}U$ ratio measurements were 80% and 180% (2*s*, *n* = 15), respectively. In contrast, much higher signal intensities for ^{238}U could be employed when the attenuator device was employed. Under optimum laser ablation conditions, the resulting signal intensities for ^{206}Pb were > 200 cps. This resulted in much better counting statistics on ^{206}Pb and ^{207}Pb isotopes.

The measured U–Pb isotope data obtained with the attenuator device is shown in Table 3. The resulting precisions of $^{206}Pb/^{238}U$ and $^{207}Pb/^{235}U$ ratio measurements were 16% and 63% (2*s*, *n* = 11), respectively, demonstrating improved values (Figure 4b). Despite the obvious success in obtaining better precision in the isotope ratio measurements, we found in fact that almost all the data plotted in Figure 4b systematically deviate from the concordia curve (the average of concordance values was about 295%, where perfect concordance of $^{206}Pb/^{238}U$ and $^{207}Pb/^{235}U$ ages would be 100%), representing the isotopic growth of the $^{206}Pb/^{238}U$ and $^{207}Pb/^{235}U$ ratios in a closed system. The clear offset of the data points from the concordia curve could be explained by the improper correction of the background, since the conventional gas blank correction was made in this case (Figure 4b). This is well demonstrated by the resulting U–Pb isotope data shown in Figure 4c. With both the attenuator device and the background correction based on an ablation blank using the synthesised zircon, the measured $^{206}Pb/^{238}U$ and $^{207}Pb/^{235}U$ ratios for the OGPK zircons fell close to a concordia curve with an average concordance of *ca.* 129%. This indicates that reliable background correction can be made by the ablation blank procedure using the synthesised zircon.

The effect of the attenuator device and the background correction based on the ablation blank using synthesised zircon was also demonstrated from U–Pb isotopic data obtained from the Bishop Tuff and Kirigamine zircons (Table 4 and Figure 5). For the Bishop Tuff zircon, the precisions of the $^{206}Pb/^{238}U$ and $^{207}Pb/^{235}U$ ratio measurements obtained without the attenuator were 17% and 104%, respectively (2*s*, *n* = 7). With the attenuator, the precisions of the measurements were improved dramatically to 4.4% for $^{206}Pb/^{238}U$ and 21% for $^{207}Pb/^{235}U$ ratios (2*s*, *n* = 7). For the Kirigamine zircons, the precisions of the $^{206}Pb/^{238}U$ and $^{207}Pb/^{235}U$ ratio measurements obtained without the attenuator were 25% and 88%, respectively (2*s*, *n* = 7), but were 2.1% for $^{206}Pb/^{238}U$ and 9.2% for $^{207}Pb/^{235}U$ (2*s*, *n* = 7) with the device, suggesting significant improvement. For the OGPK zircons, the measured $^{206}Pb/^{238}U$ and $^{207}Pb/^{235}U$ ratios varied significantly when no attenuator was used. This was mainly due to poor counting statistics on ^{206}Pb and ^{207}Pb. With the attenuator, the overall variation for the $^{206}Pb/^{238}U$ and $^{207}Pb/^{235}U$ ratios became dramatically smaller than that obtained without the attenuator. Moreover, with both the attenuator and the ablation blank, the average percentage concordance values were 148% for the Bishop Tuff and 117% for the Kirigamine zircons. These values are significantly

Table 3.
U-Pb isotopic data for OGPK zircons obtained with and without attenuation

Spot ID	Detector	Blank	Measured count rate (cps)					Isotopic ratios*1			Age (Ma)		Conc. (%)
			^{204}Pb	^{206}Pb	^{207}Pb	^{238}U*2	^{235}U	^{207}Pb/ ^{206}Pb	^{206}Pb/ ^{238}U	^{207}Pb/ ^{235}U	^{206}Pb/^{238}U	^{207}Pb/^{235}U	
Without attenuator, with gas blank													
OGPK-1–1	Attenuator	Gas	-10	68	19	432423	3136	0.2736 ± 0.0042	0.00017 ± 0.000041	0.0063 ± 0.0029	1.1 ± 0.3	6 ± 3	586
OGPK-1–3	disabled	blank	-16	77	2	446036	3235	0.0311 ± 0.0005	0.00018 ± 0.000042	0.0008 ± 0.0010	1.2 ± 0.3	1 ± 1	67
OGPK-1–7			14	72	32	455412	3303	0.4472 ± 0.0069	0.00017 ± 0.000040	0.0104 ± 0.0037	1.1 ± 0.3	10 ± 4	956
OGPK-1–8			-10	55	16	345581	2506	0.2946 ± 0.0045	0.00017 ± 0.000046	0.0069 ± 0.0034	1.1 ± 0.3	7 ± 3	631
OGPK-1–11			-32	47	23	424602	3080	0.4925 ± 0.0076	0.00012 ± 0.000035	0.0080 ± 0.0033	0.8 ± 0.2	8 ± 3	1054
OGPK-1–14			-25	64	16	407513	2956	0.2524 ± 0.0039	0.00017 ± 0.000042	0.0058 ± 0.0029	1.1 ± 0.3	6 ± 3	541
OGPK-1–15			10	56	1	408931	2966	0.0221 ± 0.0003	0.00015 ± 0.000039	0.0004 ± 0.0008	0.9 ± 0.3	0 ± 1	48
OGPK-1–16			47	22	17	318868	2313	0.8028 ± 0.0124	0.00007 ± 0.000031	0.0080 ± 0.0038	0.5 ± 0.2	8 ± 4	1718
OGPK-1–18			11	109	45	339269	2461	0.4123 ± 0.0064	0.00034 ± 0.000066	0.0194 ± 0.0058	2.2 ± 0.4	19 ± 6	878
OGPK-1–19			-68	75	10	408284	2961	0.1401 ± 0.0022	0.00020 ± 0.000045	0.0037 ± 0.0023	1.3 ± 0.3	4 ± 2	301
OGPK-1–20			-41	97	50	388700	2819	0.5142 ± 0.0079	0.00027 ± 0.000054	0.0187 ± 0.0053	1.7 ± 0.4	19 ± 5	1095
OGPK-1–21			-51	32	5	372674	2703	0.1469 ± 0.0023	0.00009 ± 0.000033	0.0018 ± 0.0017	0.6 ± 0.2	2 ± 2	316
OGPK-1–22			-5	52	0	386550	2804	0.0017 ± 0.00003	0.00014 ± 0.000040	0.0000 ± 0.0002	0.9 ± 0.3	0 ± 0	4
OGPK-1–24			-12	41	7	333726	2420	0.1700 ± 0.0026	0.00013 ± 0.000041	0.0031 ± 0.0023	0.9 ± 0.3	3 ± 2	365
OGPK-1–26			-32	44	15	359331	2606	0.3461 ± 0.0053	0.00013 ± 0.000039	0.0061 ± 0.0032	0.8 ± 0.3	6 ± 3	742
With attenuator, gas blank baseline													
OGPK 7–2	Attenuated	Gas	55	243	41	1220019	8848	0.1705 ± 0.0031	0.00020 ± 0.000026	0.0046 ± 0.0014	1.28 ± 0.17	4.7 ± 1.5	365
OGPK 7–3	for ^{238}U	blank	51	208	37	1135963	8239	0.1799 ± 0.0033	0.00018 ± 0.000026	0.0045 ± 0.0015	1.17 ± 0.17	4.5 ± 1.5	385
OGPK 7–4			-3	202	37	1163363	8438	0.1852 ± 0.0034	0.00017 ± 0.000025	0.0044 ± 0.0014	1.11 ± 0.16	4.4 ± 1.5	396
OGPK 7–6			67	366	37	2041180	14804	0.1023 ± 0.0019	0.00018 ± 0.000020	0.0025 ± 0.0008	1.15 ± 0.13	2.5 ± 0.8	219
OGPK 7–7			1	187	29	911193	6609	0.1574 ± 0.0029	0.00020 ± 0.000031	0.0044 ± 0.0016	1.32 ± 0.20	4.4 ± 1.6	337
OGPK 7–8			-27	174	25	838123	6079	0.1462 ± 0.0027	0.00021 ± 0.000032	0.0041 ± 0.0016	1.33 ± 0.21	4.2 ± 1.7	313
OGPK 7–9			-6	432	39	2422073	17567	0.0913 ± 0.0017	0.00018 ± 0.000018	0.0022 ± 0.0007	1.14 ± 0.12	2.2 ± 0.7	196
OGPK 7–12			-77	1421	89	8660355	62811	0.0630 ± 0.0012	0.00016 ± 0.000011	0.0014 ± 0.0003	1.05 ± 0.07	1.4 ± 0.3	135
OGPK 7–13			36	239	39	1415889	10269	0.1650 ± 0.0030	0.00017 ± 0.000023	0.0038 ± 0.0012	1.08 ± 0.15	3.8 ± 1.2	353
OGPK 7–14			46	279	31	1625233	11787	0.1127 ± 0.0021	0.00017 ± 0.000021	0.0026 ± 0.0009	1.10 ± 0.14	2.7 ± 1.0	241
OGPK 7–15			-46	245	34	1319863	9573	0.1405 ± 0.0026	0.00018 ± 0.000025	0.0035 ± 0.0012	1.19 ± 0.16	3.6 ± 1.2	301
With attenuator, ablation blank baseline													
OGPK 7–2	Attenuated	Ablation	56	221	20	1220022	8848	0.0907 ± 0.0017	0.00018 ± 0.000025	0.0022 ± 0.0010	1.16 ± 0.16	2.2 ± 1.0	194
OGPK 7–3	for ^{238}U	blank*3	52	186	16	1135966	8239	0.0862 ± 0.0016	0.00016 ± 0.000025	0.0019 ± 0.0010	1.05 ± 0.16	1.9 ± 1.0	185
OGPK 7–4			-2	180	16	1163366	8438	0.0891 ± 0.0016	0.00015 ± 0.000024	0.0019 ± 0.0009	0.99 ± 0.15	1.9 ± 0.9	191
OGPK 7–6			67	344	16	2041183	14804	0.0466 ± 0.0009	0.00017 ± 0.000019	0.0011 ± 0.0005	1.08 ± 0.12	1.1 ±0.5	100
OGPK 7–7			2	165	8	911196	6609	0.0486 ± 0.0009	0.00018 ± 0.000029	0.0012 ± 0.0008	1.16 ± 0.19	1.2 ± 0.9	104
OGPK 7–8			-26	152	4	838126	6079	0.0264 ± 0.0005	0.00018 ± 0.000030	0.0006 ± 0.0006	1.16 ± 0.19	0.7 ± 0.7	57
OGPK 7–9			-5	410	18	2422076	17567	0.0440 ± 0.0008	0.00017 ± 0.000018	0.0010 ± 0.0005	1.08 ± 0.11	1.0 ± 0.5	94
OGPK 7–12			-77	1399	68	8660358	62811	0.0486 ± 0.0009	0.00016 ± 0.000010	0.0011 ± 0.0003	1.03 ± 0.07	1.1 ± 0.3	104
OGPK 7–13			37	217	18	1415892	10269	0.0831 ± 0.0015	0.00015 ± 0.000021	0.0017 ± 0.0008	0.98 ± 0.14	1.7 ± 0.8	178
OGPK 7–14			47	257	10	1625236	11787	0.0390 ± 0.0007	0.00016 ± 0.000020	0.0008 ± 0.0005	1.01 ± 0.13	08 ± 0.5	84
OGPK 7–15			-46	223	13	1319866	9573	0.0584 ± 0.0011	0.00017 ± 0.000023	0.0013 ± 0.0007	1.08 ± 0.15	1.4 ± 0.8	125

*1 Uncertainties are 2s.

*2 Corrected count rate from measured count rate based on the attenuation gain.

*3 Synthesised zircon was employed for the ablation blank measurements.

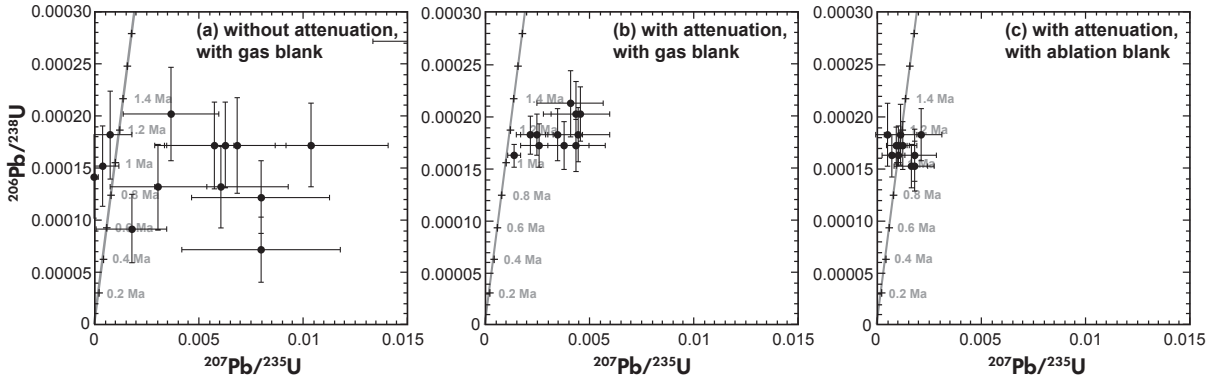

Figure 4. Measured $^{206}Pb/^{238}U$ and $^{207}Pb/^{235}U$ ratios for OGPK zircons.

Table 4.
U-Pb isotope data for Bishop Tuff and Kirigamine 03 zircons obtained with and without attenuator device

Sample	Spot	Detector	$^{206}Pb/^{238}U$*	%Err	$^{207}Pb/^{235}U$*	%Err	Age (Ma)		Conc. (%)
							$^{206}Pb/^{238}U$*	$^{207}Pb/^{235}U$*	
(1) Bishop Tuff	Spot 1	Without	0.00011375 ± 0.00001468	12.9	0.000473 ± 0.0003515	74	0.733 ± 0.095	0.48 ± 0.36	65
	Spot 2		0.00012580 ± 0.00001578	12.5	0.002131 ± 0.0007634	36	0.811 ± 0.102	2.16 ± 0.77	267
	Spot 3		0.00011905 ± 0.00001490	12.5	0.001173 ± 0.0005495	47	0.767 ± 0.096	1.19 ± 0.56	155
	Spot 4		0.00010853 ± 0.00001437	13.2	0.001589 ± 0.0006459	41	0.700 ± 0.093	1.61 ± 0.65	230
	Spot 5		0.00011101 ± 0.00001415	12.7	0.002625 ± 0.0008088	31	0.716 ± 0.091	2.66 ± 0.82	372
	Spot 6		0.00011223 ± 0.00001519	13.5	0.001293 ± 0.0006058	47	0.723 ± 0.098	1.31 ± 0.61	181
	Spot 7		0.00013617 ± 0.00001590	11.7	0.003152 ± 0.0008999	29	0.878 ± 0.103	3.20 ± 0.91	364
	Spot 1	Attenuated	0.00010855 ± 0.00000413	3.8	0.0009979 ± 0.0001433	14	0.700 ± 0.027	1.01 ± 0.15	145
	Spot 2	for ^{238}U	0.00011130 ± 0.00000430	3.9	0.0009268 ± 0.0001417	15	0.717 ± 0.028	0.94 ± 0.14	
	Spot 3	signal	0.00011119 ± 0.00000439	3.9	0.0010738 ± 0.0001558	15	0.717 ± 0.028	1.09 ± 0.16	152
	Spot 4		0.00011046 ± 0.00000425	3.8	0.0009817 ± 0.0001448	15	0.712 ± 0.027	1.00 ± 0.15	140
	Spot 5		0.00011450 ± 0.00000422	3.7	0.0012019 ± 0.0001562	13	0.738 ± 0.027	1.22 ± 0.16	165
	Spot 6		0.00011503 ± 0.00000564	4.9	0.0012096 ± 0.0002090	17	0.742 ± 0.036	1.23 ± 0.21	166
	Spot 7		0.00011428 ± 0.00000483	4.2	0.0009875 ± 0.0001623	16	0.737 ± 0.031	1.00 ± 0.16	136
(2) Kirigamine 03	Spot 1	Without	0.0001686 ± 0.0000212	12.6	0.003420 ± 0.001123	32.8	1.087 ± 0.137	3.47 ± 1.14	319
	Spot 2		0.0001806 ± 0.0000238	13.2	0.001108 ± 0.000693	62.5	1.164 ± 0.153	1.12 ± 0.70	97
	Spot 3		0.0002252 ± 0.0000264	11.7	0.003343 ± 0.001198	35.8	1.451 ± 0.170	3.39 ± 1.21	233
	Spot 4		0.0001681 ± 0.0000227	13.5	0.004973 ± 0.001451	29.2	1.084 ± 0.146	5.04 ± 1.46	465
	Spot 5		0.0001699 ± 0.0000226	13.3	0.003131 ± 0.001141	36.4	1.095 ± 0.146	3.17 ± 1.15	290
	Spot 6		0.0002120 ± 0.0000281	13.2	0.004642 ± 0.001546	33.3	1.367 ± 0.181	4.70 ± 1.56	344
	Spot 7		0.0001731 ± 0.0000219	12.7	0.001747 ± 0.000819	46.9	1.116 ± 0.141	1.77 ± 0.83	159
	Spot 1	Attenuated	0.0001480 ± 0.00000177	1.2	0.001159 ± 0.0000562	4.8	0.954 ± 0.011	1.18 ± 0.06	123
	Spot 2	for ^{238}U	0.0001479 ± 0.00000183	1.2	0.001097 ± 0.0000564	5.1	0.953 ± 0.012	1.11 ± 0.06	117
	Spot 3	signal	0.0001483 ± 0.00000198	1.3	0.001161 ± 0.0000628	5.4	0.956 ± 0.013	1.18 ± 0.06	123
	Spot 4		0.0001463 ± 0.00000194	1.3	0.001090 ± 0.0000599	5.5	0.943 ± 0.012	1.11 ± 0.06	117
	Spot 5		0.0001481 ± 0.00000144	1.0	0.001026 ± 0.0000428	4.2	0.955 ±0.009	1.04 ± 0.04	109
	Spot 6		0.0001459 ± 0.00000146	1.0	0.001070 ± 0.0000449	4.2	0.940 ± 0.009	1.09 ± 0.05	116
	Spot 7		0.0001441 ± 0.00000167	1.2	0.001058 ± 0.0000512	4.8	0.929 ± 0.011	1.07 ± 0.05	116

* Uncertainties were calculated based on the counting statistics (2s).

better than those obtained without the attenuator, together with the conventional gas blank corrections (230% for the Bishop Tuff and 270% for Kirigamine).

$^{206}Pb/^{238}U$ and $^{207}Pb/^{235}U$ ratio values measured for the Bishop Tuff and Kirigamine zircons using both the attenuator and ablation blank show some discordance that could be due to very small Pb losses after crystallisation. The discordance could also be due to a contribution of initial

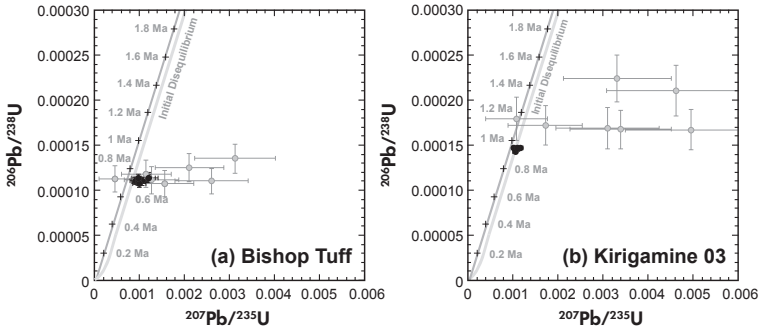

Figure 5. Measured $^{206}Pb/^{238}U$ and $^{207}Pb/^{235}U$ ratios for zircons of the Bishop Tuff and Kirigamine. The curve labelled 'initial disequilibrium' represents the corrected concordia curve based on a D^{Th}/D^{U} value of 0.19 (Crowley *et al.* 2007) and a D^{Pa}/D^{U} value of 0.9–2.2 (Schmitt 2007).

disequilibrium of ^{230}Th and ^{231}Pa (Schärer 1984, Pickett and Murrell 1997). The concordia plots given in Figures 4 and 5 are based on two assumptions: (a) maintenance of U–Pb system closure, (b) isotopic equilibrium during the crystallisation of zircons from source melts. However, this is not the case for the U–Pb age determination of young (~ 1 Ma) zircons. When initial disequilibrium is taken into the account, the zircons should shift towards lower $^{206}Pb/^{238}U$ and higher $^{207}Pb/^{235}U$ ratios on the concordia curves (Figures 5a and b). The magnitude of the disequilibrium on the ^{238}U- and ^{235}U-decay series can be estimated by the distribution ratio of Th, Pa and U between zircon and source melt (D^{Th}/D^{U} and D^{Pa}/D^{U}). With a D^{Th}/D^{U} ratio of 0.19 (Crowley *et al.* 2007) and D^{Pa}/D^{U} = 0.9–2.2 (Schmitt 2007), all the U–Pb isotopic data for zircon obtained in this study fall close to the concordia curve after the correction of the initial disequilibrium. This demonstrates that the resulting U–Pb isotopic data for both the Bishop Tuff and Kirigamine zircons are close to concordant when the initial disequilibrium ^{230}Th and ^{231}Pa is taken into account.

U–Pb isotope data from the Bishop Tuff and Kirigamine zircons, show that the resulting signal intensities for ^{206}Pb and ^{207}Pb isotopes are significantly higher than those found from OGPK zircons (i.e., ^{206}Pb > 3000 cps, ^{207}Pb > 300 cps for Bishop Tuff; ^{206}Pb > 5000 cps, ^{207}Pb > 500 cps for Kirigamine). This is mainly due to high U content in zircons from the Bishop Tuff and Kirigamine. Because of the elevated signal intensities for ^{206}Pb and ^{207}Pb isotopes, the contribution of the small changes in background counts obtained with and without laser ablation did not affect the measured $^{206}Pb/^{238}U$ and $^{207}Pb/^{235}U$ ratios. Nevertheless, because the U contents for most zircons is in the range 100–400 μg g^{-1}, their signal intensities for ^{206}Pb and ^{207}Pb isotopes would be much lower than those found in Bishop Tuff and Kirigamine zircons. The combination of ablation blank corrections and use of the attenuator device could provide a powerful technique to obtain reliable U–Pb age data from zircons of ~ 1 Ma and younger by LA-ICP-MS.

Conclusions

Measured $^{206}Pb/^{238}U$ and $^{207}Pb/^{235}U$ ratios for young zircons are < 0.00005. Thus, limitations in counting statistics for ^{206}Pb and ^{207}Pb signals and erroneous measurement of signal intensity for ^{238}U, due to improper correction for the dead time, could cause poor linearity in $^{206}Pb/^{238}U$ and $^{207}Pb/^{235}U$ ratio measurements by LA-ICP-MS. For U–Pb age determinations of young zircons, both proper correction for the background counts for ^{206}Pb and ^{207}Pb isotopes and use of an attenuator device can improve data accuracy and precision. The data obtained here demonstrate clearly that this new LA-ICP-MS technique could become a significant one for the U–Pb age determination of young zircons.

Acknowledgements

We are grateful to Prof. Paul Sylvester (Memorial University, Canada) for much advice and constructive comments on the manuscript. We are also grateful to Drs. Yuji Orihashi (Earthquake Research Institute, The University of Tokyo, Japan), Tsuyoshi Iizuka (The University of Tokyo, Japan), Kenshi Maki (Akita University, Japan) and Mr. Yugo Danhara (Kyoto Fission-Track Co.) for scientific advice and technical support. The sample of volcanic rock from Unzen was kindly provided by Dr. Yoshihiko Goto (Muroran Institute of Technology). Synthesised zircons used in this study were kindly provided by Dr. Noriko Hasebe (Kanazawa University, Japan). This work was supported by a Grant-in-Aid for Scientific Research (S21224013) to TH from the Ministry of Education, Culture, Sports, Science and Technology, Japan.

References

Autrique D., Bogaerts A., Lindner H., Garcia C.C. and Niemax K. (2008)
Design analysis of a laser ablation cell for inductively coupled plasma-mass spectrometry by numerical simulation. Spectrochimica Acta, Part B, 63, 257–270.

Bühn B., Pimentel M.M., Matteini M. and Dantas E.L. (2009)
High spatial resolution analysis of Pb and U isotopes for geochronology by laser ablation multi-collector inductively coupled plasma-mass spectrometry (LA-MC-ICP-MS). Anais da Academia Brasileira de Ciências, 81, 1.

Chase A.B. and Osmer J.A. (1966)
Growth and preferential doping of zircon and thorite. Journal of the Electrochemical Society, 113, 198–199.

Chew D.M., Petrus J.A. and Kamber B.S. (2014)
U-Pb LA-ICP-MS dating using accessory mineral standards with variable common Pb. Chemical Geology, 363, 185–199.

Cowan G.A. and Adler H.H. (1976)
The variability of the natural abundance of ^{235}U. Geochimica et Cosmochimica Acta, 40, 1487–1490.

Crowley J.L., Schoene B. and Bowring S.A. (2007)
U-Pb dating of zircon in the Bishop Tuff at the millennial scale. Geology, 35, 1123–1126.

Danhara T., Iwano H., Kasuya M. and Yamashita T. (1993)
The PFA Sheet: An improved mounting material for fission track analysis of zircon. Nuclear Tracks and Radiation Measurements, 21, 283–285.

Danhara T., Kamata H. and Iwano H. (1997)
Fission-track ages of zircons in the Yabakei pyroclastic-flow deposit in central Kyushu and the Pink Volcanic Ash of the Osaka Group. Journal of the Geological Society of Japan, 103, 994–997.

Eggins S.M., Kinsley L.P.J. and Shelley J.M.G. (1998)
Deposition and element fractionation processes during atmospheric pressure laser sampling for analysis by ICP-MS. Applied Surface Science, 129, 278–286.

Frei D. and Gerdes A. (2009)
Precise and accurate *in situ* U-Pb dating of zircon with high sample throughput by automated LA-SF-ICP-MS. Chemical Geology, 261, 261–270.

Freydier R., Candaudap F., Poitrasson F., Arbouet A., Chatel B. and Dupré B. (2008)
Evaluation of infrared femtosecond laser ablation for the analysis of geomaterials by ICP-MS. Journal of Analytical Atomic Spectrometry, 23, 702–710.

Guillong M., Horn I. and Günther D. (2003)
A comparison of 266 nm, 213 nm and 193 nm produced from a single solid state Nd:YAG laser for laser ablation ICP-MS. Journal of Analytical Atomic Spectrometry, 18, 1224–1230.

Günther D. and Heinrich C.A. (1999)
Enhanced sensitivity in laser ablation-ICP mass spectrometry using helium-argon mixtures as aerosol carrier. Journal of Analytical Atomic Spectrometry, 14, 1363–1368.

Hildreth W. (1979)
The Bishop Tuff: Evidence for the origin of compositional zonation in silicic magma chambers. Geological Society of America Special Paper, 180, 43–75.

Hirata T. and Kon Y. (2008)
Evaluation of the analytical capability of NIR femtosecond laser ablation-inductively coupled plasma-mass spectrometry. Analytical Sciences, 24, 345–353.

Hirata T. and Nesbitt R.W. (1995)
U-Pb isotope geochronology of zircon: Evaluation of the laser probe-inductively coupled plasma-mass spectrometry technique. Geochimica et Cosmochimica Acta, 59, 2491–2500.

Hirata T., Iizuka T. and Orihashi Y. (2005)
Reduction of mercury background on ICP-mass spectrometry for *in situ* U-Pb age determinations of zircon samples. Journal of Analytical Atomic Spectrometry, 20, 696–701.

Horn I. and von Blanckenburg F. (2007)
Investigation on elemental and isotopic fractionation during 196 nm femtosecond laser ablation multiple collector inductively coupled plasma-mass spectrometry. Spectrochimica Acta Part B, 62, 410–422.

Iizuka T. and Hirata T. (2004)
Simultaneous determinations of U-Pb age and REE abundances for zircons using ArF excimer laser ablation-ICP-MS. Geochemical Journal, 38, 229–241.

Iwano H., Orihashi Y., Hirata T., Ogasawara M., Danhara T., Horie K., Hasebe N., Sueoka S., Tamura A., Hayasaka Y., Katsube A., Ito H., Tani K., Kimura J., Chang Q., Kouchi Y., Haruta Y. and Yamamoto K. (2013)
An inter-laboratory evaluation of OD-3 zircon for use as a secondary U-Pb dating standard. Island Arc, 22, 382–394.

Jackson S.E., Pearson N.J., Griffin W.L. and Belousova E.A. (2004)
The application of laser ablation-inductively coupled plasma-mass spectrometry to *in situ* U-Pb zircon geochronology. Chemical Geology, 211, 47–69.

Koch J. and Günther D. (2011)
Review of the state-of-the-art of laser ablation inductively coupled plasma-mass spectrometry. Applied Spectroscopy, 65, 155–162.

Košler J., Sláma J., Belousova E., Corfu F., Gehrels G.E., Gerdes A., Horstwood M.S.A., Sircombe K.N., Sylvester P.J., Tiepolo M., Whitehouse M.J. and Woodhead J.D. (2013)
U-Pb detrital zircon analysis – Results of an inter-laboratory comparison. Geostandards and Geoanalytical Research, 37, 243–259.

references

Pickett D.A. and Murrell M.T. (1997)
Observations of $^{231}Pa/^{235}U$ disequilibrium in volcanic rocks. **Earth and Planetary Science Letters**, **148**, 259–271.

Poitrasson F., Mao X., Mao S.S., Freydier R. and Russo R.E. (2003)
Comparison of ultraviolet femtosecond and nanosecond laser ablation-inductively coupled plasma-mass spectrometry analysis in glass, monazite and zircon. **Analytical Chemistry**, **75**, 6184–6190.

Sarna-Wojcicki A.M., Pringle M.S. and Wijbrans J. (2000)
New $^{40}Ar/^{39}Ar$ age of the Bishop Tuff from multiple sites and sediment rate calibration for the Matuyalna-Brunhes boundary. **Journal of Geophysical Research**, **105**, 431–443.

Schärer U. (1984)
The effect of initial ^{230}Th disequilibrium on young U-Pb ages: The Makalu case, Himalaya. **Earth and Planetary Science Letters**, **67**, 191–204.

Schmitt A.K. (2007)
Ion microprobe analysis of $(^{231}Pa)/(^{235}U)$ and an appraisal of protactinium partitioning in igneous zircon. **American Mineralogist**, **92**, 691–694.

Sugihara S., Nagai M., Shibata T., Danhara T. and Iwano H. (2009)
Petrographic and geochemical study and fission-track dating of obsidian from the Kirigamine and Kitayatsugatake areas in the central part of Japan: The fundamental research for sourcing of obsidian artifacts. **Sundai Historical Review**, **136**, 57–109.

Tunheng A. and Hirata T. (2004)
Development of signal smoothing device for precise elemental analysis using laser ablation-ICP-mass spectrometry. **Journal of Analytical Atomic Spectrometry**, **19**, 932–934.

Wiedenbeck M., Allé P., Corfu F., Griffin W.L., Meier M., Oberli F., von Quadt A., Roddick J.C. and Spiegel W. (1995)
Three natural zircon standards for U-Th-Pb, Lu-Hf, trace element and REE analyses. **Geostandards Newsletter**, **19**, 1–23.